Patient-Derived Xenograft and Cell Line Models of Human Primary Cutaneous Diffuse Large B-Cell Lymphoma-Leg Type

Martina Prochazkova-Carlotti, Audrey Gros, Elodie Richard, Floriane Cherrier, Elodie Laharanne, Yamina Idrissi, Camille Baron, Sandrine Poglio, Océane Ducharme, Sarah Menguy, et al.

Patient-Derived Xenograft and Cell Line Models of Human Primary Cutaneous Diffuse Large B-Cell Lymphoma-Leg Type

JID Open

Journal of Investigative Dermatology (2022) ■, ■–■; doi:10.1016/j.jid.2022.08.043

TO THE EDITOR

Primary cutaneous diffuse large B-cell lymphoma, leg-type (PCDLBCL-LT) is a rare and aggressive malignancy, mostly occurring on the leg of elderly women (Willemze et al., 2019). PCDLBCL-LT harbors an activated B-cell–like diffuse large B-cell lymphoma (ABC-DLBCL) signature and is enriched for mutations involving the toll-like receptor, B-cell receptor, and NF-κB pathways (Pham-Ledard et al., 2012; Zhou et al., 2018). The high frequency of *MYD88*^{L265P} mutation in combination with those of *CD79B* and *PIM1* relates these lymphomas to the MCD/C5 subset of diffuse large B-cell lymphomas, which includes ABC-DLBCL occurring in extranodal sites (Danilov et al., 2022). The combination of rituximab and age-adapted polychemotherapy has improved the prognosis of patients, but refractory disease or relapse occurs in about half of patients. The lack of an experimental model impaired functional studies to decipher PCDLBCL-LT biology and therapeutic resistance mechanisms. In this study, we report the successful expansion of cutaneous B lymphoma cells, thanks to a patient-derived xenograft (PDX), followed by the establishment of a stable PCDLBCL-LT cell line.

An explant of a skin biopsy from a leg tumor in an untreated woman aged 85 years with PCDLBCL-LT was subcutaneously transplanted in female immunodeficient NSG (NOD.Cg-Prkdc[scid] Il2rg[tm1Wjll]/SzJ) mouse. Previously, the patient provided written informed consent in accordance with the Declaration of Helsinki and national ethics rules, and the ethical research committee of Bordeaux approved the manipulation of PCDLBCL-LT samples (CER-BDX-2022-18). Engraftment, as a nodule, appeared on day 42, and then it grew exponentially until the mouse killed on day 73 showing a brownish and hemorrhagic subcutaneous tumor without ulceration (Figure 1a). After tumor dissociation, flow cytometry analysis revealed that almost all isolated cells (>98%) expressed CD19, CD20, and CD45, confirming their human B-cell origin (Supplementary Figure S1a). An autopsy revealed splenomegaly, and extracutaneous spreading was confirmed using anti–HLA-ABC staining in the skin, femur, spleen, kidney, and liver (Figure 1b), as reported at advanced stages of the disease in some patients (Zinzani et al., 2006). To establish PCDLBCL-LT cell line, fresh cells isolated from the xenograft were grown for 45 days in a culture medium containing a cocktail of cytokines (CD40L, IL-2, IL-4, and IL-10), which were thereafter gradually removed (Supplementary Materials and Methods). Then, cells were routinely expanded in RPMI supplemented with fetal bovine serum and human AB serum. These so-called ARSI cells grew in suspension as more or less big clumps with a mean doubling time of about 24 hours (Supplementary Figure S1b and 1c). A continuous expansion for >1 year was achieved with >200 proliferation doublings, suggesting ARSI cell line immortalization (Sugimoto et al., 2004). Clonality of the Ig genes of the PDX and ARSI cell line, assessed by the BIOMED-2 protocol, showed the same heavy and light chain Ig genes monoclonal rearrangements as in the patient's tumor cells (Supplementary Figure S1d). Immunophenotypes of PDX and ARSI cell line were compared with those of the original tumor (Figure 1c). Patient tumor cells were positive for CD20, BCL2, MUM1, IgM, and BCL6^{low} and negative for CD10, CD30, and IgG, with MYC and Ki-67 expressions in about 60 and 70% of cells, respectively, consistent with an activated B-cell phenotype. PDX cells and ARSI cell line displayed a phenotype similar to that of the initial biopsy, which was stable with time in culture.

Next, we analyzed the genetic status of the patient tumor and compared it with that of the ARSI cell line. FISH showed the absence of *MYC* rearrangement both in patients and in cell line. SNP array and multicolor FISH showed a poorly rearranged genomic profile of the patient tumor cells. This profile remained stable along culture time except for the number of chromosomes X (disomy or monosomy) and 18 (trisomy or tetrasomy) and for copy-neutral loss of heterozygosity at chromosome 7 (Figure 2a–c and Supplementary Table S1). Next-generation sequencing with a dedicated panel (Mareschal et al., 2017) revealed mutations of *MYD88*, *CD79B*, and *PIM1* genes (Supplementary Table S2) in the patient tumor, corresponding to a prototypic PCDLBCL-LT genetic pattern. These mutations were retained in the ARSI cell line, with some changes for *IRF4* and *PIM1* mutations. The original *IRF4*^{H56T} mutation (allelic frequency at 20% in the patient's tumor) was lost in the PDX and in the ARSI cell line, whereas *IRF4*^{S104R} and *IRF4*^{G60K} mutations appeared at 7 and 13 months of cell culture, respectively. Of note, the second *IRF4* allele was found deleted in the patient's tumor and ARSI cell line. For *PIM1*, the

Abbreviations: ABC-DLBCL, activated B-cell–like diffuse large B-cell lymphoma; PCDLBCL-LT, primary cutaneous diffuse large B-cell lymphoma, leg-type; PDX, patient-derived xenograft

Accepted manuscript published online XXX; corrected proof published online XXX

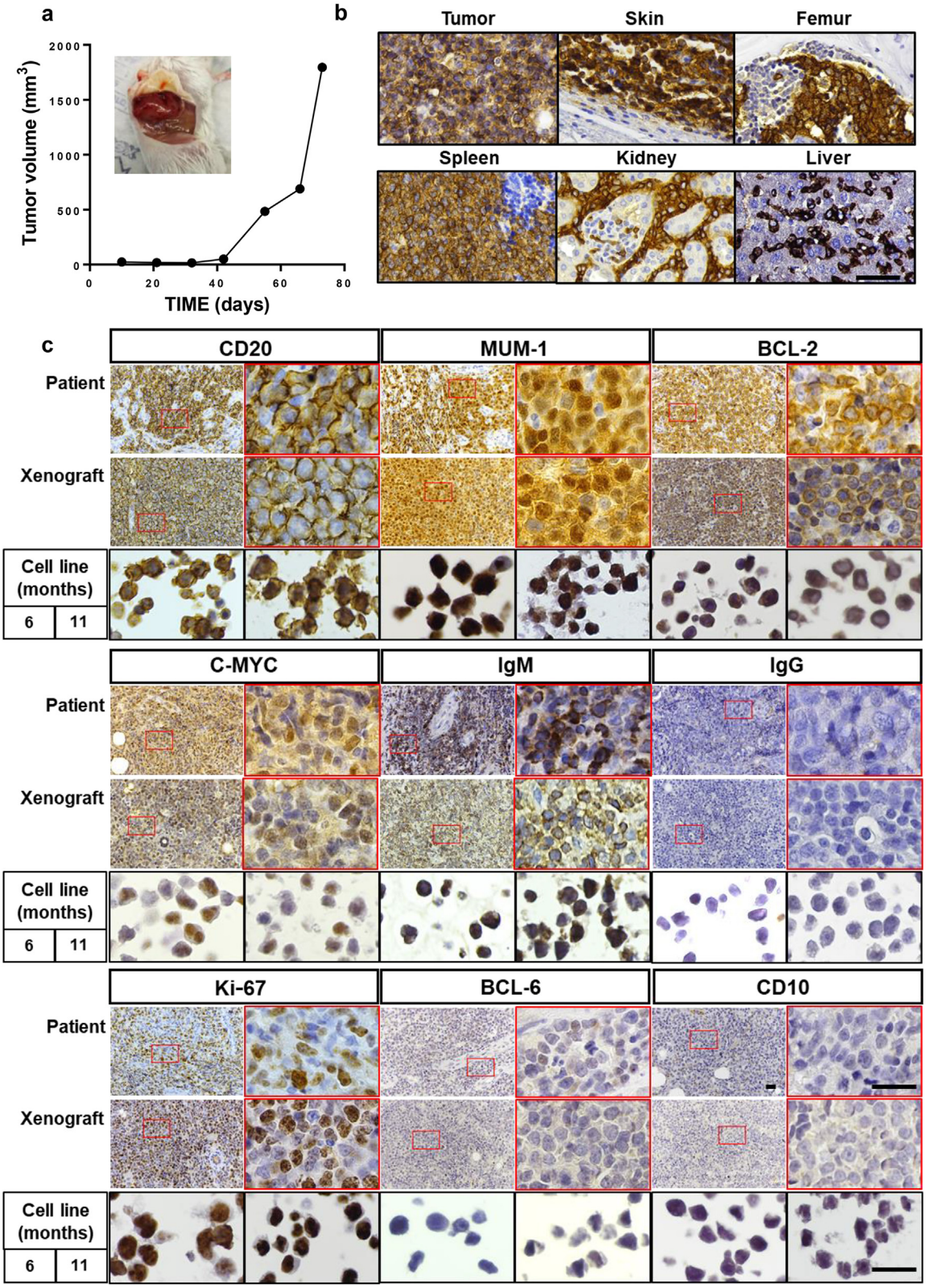

Figure 1. Characterization of the PCDLBCL-LT PDX and the ARSI cell line. **(a)** A piece of the fresh biopsy was subcutaneously grafted in NSG (NOD.Cg-Prkdc [scid]Il2rg[tm1Wjll]/SzJ) immunodeficient mouse. Tumor volume curve was established until the mouse was killed when the tumor reached approximately 2,000 mm^3. Insert shows the appearance of the subcutaneous tumor at dissection. (**b**) Identification of human cells by detection of HLA-ABC−positive cells using immunohistochemistry in tumor, skin, femur, spleen, kidney, and liver. Bar = 50 μm. (**c**) Immunostainings for CD20, MUM-1, BCL2, MYC, IgM, IgG, Ki67, BCL6, and CD10 in patient biopsy, PDX, and ARSI cell line after various times in culture. Note the stable phenotype between the models and the original tumor. Bar = 25 μm. PCDLBCL-LT, primary cutaneous diffuse large B-cell lymphoma, leg-type; PDX, patient-derived xenograft.

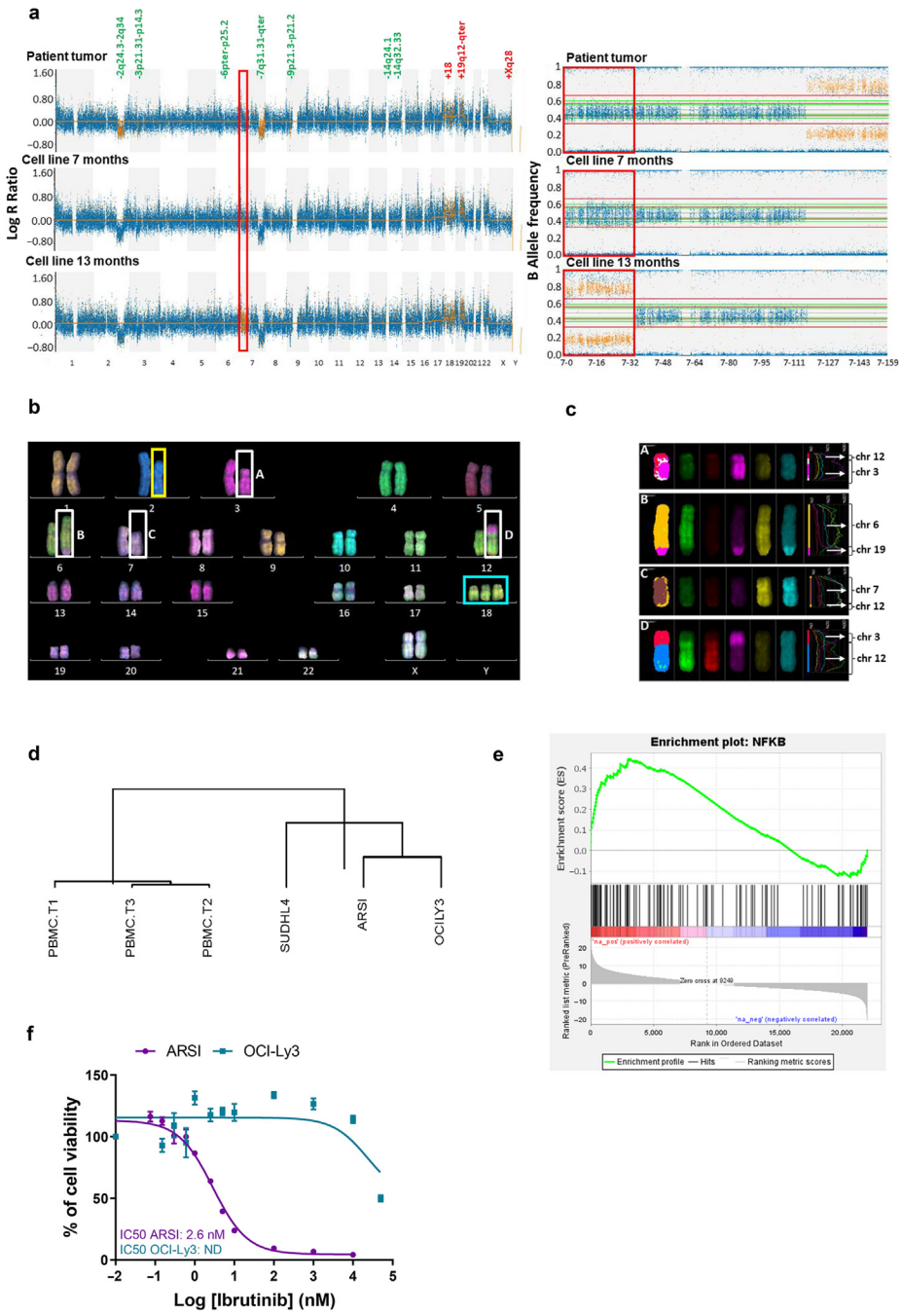

Figure 2. Genetic characterization of the ARSI cell line. (**a**) Comparison of the log R ratio of the SNP array profiles of the patient's original tumor and cell line according to time in the culture. The profiles are quite similar, exhibiting the same chromosomal abnormalities except for the copy number loss of heterozygosity (red frame) identified on the B allele frequency graph on the short arm of chromosome 7. (**b**) Multiplex FISH karyotype image of ARSI cell line showing four interchromosome rearrangements (white frames A, B, C, and D), chromosome 2 deletion (2q) (yellow frame), and chromosome 18 trisomy (cyan frame). (**c**) Fluorochrome profiles of rearranged chromosomes (white frames in **b**) with the identification of chromosomes present in translocation. (**d**) RNA-sequencing data analysis by unsupervised clustering of three cell lines (ARSI, SUDHL4, and OCI-LY3) and control PBMCs of the top 1,000 most divergent genes showed three distinct clusters. SUDHL4 is a germinal center B-cell cell line, and OCI-Ly3 is an activated B-cell cell line. (**e**) Enrichment plot of NF-κB pathway signature. ES = 0.45, NES = 1.97, and FDR < 0.005. NF-κB pathway gene list was defined as described in Supplementary Materials and Methods. (**f**) Effect of ibrutinib on ARSI and OCI-Ly3 cell viability. Cell cytotoxicity of ibrutinib was measured after 72 h using Cell titer Glo cell viability assay. The data represent the mean ± standard error of three independent experiments. IC50 was calculated using Graphpad Prism software (Graphpad Software, San Diego, CA). chr, chromosome; ES, enrichment score; FDR, false discovery rate; h, hour; IC50, half-maximal inhibitory concentration; NES, normalized enrichment score.

original tumor exhibited five mutations recovered in the PDX and ARSI cell line, and an additional mutation ($PIM1^{D226K}$) appeared in the cell line (Supplementary Table S2). Interestingly, most *IRF4* and some *PIM1* mutations occurred at DGYW/WRCH sites, which are preferential targets of the activation-induced cytidine deaminase enzyme (Rogozin and Pavlov, 2006). Our sequential data confirm ongoing aberrant somatic hypermutation of *IRF4* and

PIM1 genes, which are targets of a sustained activation-induced cytidine deaminase activity previously identified in primary cutaneous large B-cell lymphoma, leg type (Dijkman et al., 2006). Because *IRF4* and *PIM1* are respectively involved in the activation of the B-cell receptor and NF-κB signaling pathways (Maffei et al., 2021; Nihira et al., 2010), such mutational changes may contribute to the selection of a subclone with an advantage for cell immortalization or proliferation. Our lymphopanel analysis cannot exclude that aberrant somatic hypermutation also targeted other relevant oncogenes. The gene expression profile of the ARSI cell line was evaluated by RNA sequencing along with those of the SU-DHL-4 and OCI-Ly3 cell lines used as prototypic germinal center B-cell–like diffuse large B-cell lymphomas and ABC-DLBCL, respectively. As expected, unsupervised clustering analysis revealed that the ARSI cell line was classified into ABC-DLBCL together with the OCI-Ly3 cell line profile (Figure 2d). To identify the molecular pathways activated in the ARSI cell line, we compared its gene expression profile signature with that of healthy PBMC controls. Gene set enrichment analysis showed an enrichment of genes related to cell proliferation and NF-κB in the ARSI cell line (Figure 2e), in agreement with their high proliferation rate and the PCDLBCL-LT signature. These data provide evidence that the PDX cells and ARSI cell line largely capture and retain the phenotypic and genomic features of the most common PCDLBCL-LT subtype.

The rate of progression or relapse of patients after rituximab and age-adapted polychemotherapy underscore the need of selecting and evaluating new therapeutic strategies. In patients with PCDLBCL-LT, this has been hampered by the advanced age of patients and the rarity of this aggressive disease, making clinical trials difficult. In such instances, the development of preclinical models may offer an opportunity for drug screening. Ibrutinib, a Bruton tyrosine kinase inhibitor, was found effective in ABC-DLBCL cases with combined *MYD88* and *CD79A/B* mutations (Wilson et al., 2015). We therefore tested the cytotoxic effect of ibrutinib (range = 0.15–50.10^3 nM) on the ARSI cell line after 72 hours and compared it with the effect on the ABC-DLBCL nodal OCI-Ly3 cell line carrying the *MYD88*^{L265P} mutation. We observed that ARSI cells were more sensitive to ibrutinib (half-maximal inhibitory concentration = 2.6 nM) than OCI-Ly3 cells, for which the half-maximal inhibitory concentration could not be determined under our conditions (Figure 2f). Although *PIM1* mutations have been proposed to contribute to ibrutinib resistance (Kuo et al., 2016), both cell lines expressed *PIM1* mutations. More interestingly, *CARD11*, a scaffold protein that interacts with BCL10 and MALT1 downstream to Bruton tyrosine kinase and spleen tyrosine kinase to activate NF-κB signaling, is mutated in the OCI-Ly3 (*CARD11*^{L251P}) but not in the ARSI cell line. This mutation occurring in the coiled–coil domain of CARD11 has been proposed as a mechanism of resistance to B-cell receptor inhibition in diffuse large B-cell lymphomas (Fox et al., 2018) and could explain the less sensitivity of OCI-Ly3 cells to ibrutinib than ARSI cells. Altogether, these data indicate that the genetic characteristics of different preclinical models may be account for drug resistance and may contribute to screening for drug efficacy.

By overcoming the difficulties of obtaining live lymphoma B cells, in this study, we succeeded to establish the PDX and cell line models recapitulating the most common PCDLBCL-LT subtype. This original cell line may contribute to deciphering the physiopathology of PCDLBCL-LT, facilitating target identification and preclinical drug screening.

Data availability statement

No dataset was generated.

ORCIDs

Martina Prochazkova-Carlotti: http://orcid.org/0000-0002-7719-7679
Audrey Gros: http://orcid.org/0000-0002-8958-3745
Elodie Richard: http://orcid.org/0000-0003-3778-1210
Floriane Cherrier: http://orcid.org/0000-0002-4181-0283
Elodie Laharanne: http://orcid.org/0000-0002-0337-3537
Yamina Idrissi: http://orcid.org/0000-0002-8654-5380
Camille Baron: http://orcid.org/0000-0002-0875-7126
Sandrine Poglio: http://orcid.org/0000-0001-8783-0709
Océane Ducharme: http://orcid.org/0000-0001-8801-2900
Sarah Menguy: http://orcid.org/0000-0002-9214-8592
Anne Pham-Ledard: http://orcid.org/0000-0003-2960-6084
Marie Beylot-Barry: http://orcid.org/0000-0001-6150-1229
Jean-Philippe Merlio: http://orcid.org/0000-0002-0305-0850
Laurence Bresson-Bepoldin: http://orcid.org/0000-0002-8829-9945

CONFLICT OF INTEREST

The authors state no conflict of interest

ACKNOWLEDGMENTS

This work was supported by INSERM, University of Bordeaux, Ligue Régionale contre le cancer (comité de Gironde), Groupe Interrégional de Recherche Clinique et Innovation- Cancéropôle Grand Sud-Ouest- Centre Hospitalier Universitaire de Bordeaux 2018/78 to AG (grant PROTEOM). The authors thank the donors for agreeing to have their cells used for research. We acknowledge Benoît Rousseau and Julien Izotte from the A2 Animal facility at Bordeaux university (Bordeaux, France) and Atika Zouine and Vincent Pitard for technical assistance at the flow cytometry facility, CNRS UMS 3427 INSEM US 005, UB'Facsility at Bordeaux University.

AUTHOR CONTRIBUTIONS

Conceptualization: MPC, AG, JPM, LBB; Funding Acquisition: AG, LBB; Investigation: MPC, EL, AG, CB, YI, SM, LBB; Methodology: ER, FC, SP, LBB; Resources: OD, APL, MBB; Supervision: LBB; Writing - Original draft preparation: MPC, AG, JPM, LBB; Writing — Review and Editing: MPC, AG, JPM, LBB

Martina Prochazkova-Carlotti[1,7], Audrey Gros[1,2,7], Elodie Richard[3], Floriane Cherrier[1], Elodie Laharanne[2], Yamina Idrissi[1], Camille Baron[1], Sandrine Poglio[1], Océane Ducharme[4], Sarah Menguy[1,5], Anne Pham-Ledard[1,4], Marie Beylot-Barry[1,4], Jean-Philippe Merlio[1,2,8] and Laurence Bresson-Bepoldin[1,6,8,*]

[1]BRIC (BoRdeaux Institute of onCology), INSERM UMR1312, Team 5, University of Bordeaux, Bordeaux, France; [2]Tumor Bank and Tumor Biology Laboratory, University Hospital of Bordeaux, Bordeaux, France; [3]BRIC (BoRdeaux Institute of onCology), INSERM UMR1312, Team 11, University of Bordeaux, Bordeaux, France; [4]Dermatology Department, University Hospital of Bordeaux, Bordeaux, France; [5]Pathology Department, University Hospital of Bordeaux, Bordeaux, France; and [6]BRIC (BoRdeaux Institute of onCology), INSERM UMR1312, Team 5, CNRS, Université de Bordeaux, Bordeaux, France
[7]These authors contributed equally to this work.
[8]These authors contributed equally to this work.
[*]Corresponding author e-mail: Laurence.bresson-bepoldin@inserm.fr

REFERENCES

Danilov AV, Magagnoli M, Matasar MJ. Translating the biology of diffuse large B-cell lymphoma into treatment. Oncologist 2022;27:57–66.

Dijkman R, Tensen CP, Buettner M, Niedobitek G, Willemze R, Vermeer MH. Primary cutaneous follicle center lymphoma and primary cutaneous large B-cell lymphoma, leg type, are both targeted by aberrant somatic hypermutation but demonstrate differential expression of AID. Blood 2006;107:4926–9.

Fox LC, Yannakou CK, Ryland G, Lade S, Dickinson M, Campbell BA, et al. Molecular mechanisms of disease progression in primary cutaneous diffuse large B-cell lymphoma, leg type during ibrutinib therapy. Int J Mol Sci 2018;19:1758.

Kuo HP, Ezell SA, Hsieh S, Schweighofer KJ, Cheung LW, Wu S, et al. The role of PIM1 in the ibrutinib-resistant ABC subtype of diffuse large B-cell lymphoma. Am J Cancer Res 2016;6:2489–501.

Maffei R, Fiorcari S, Benatti S, Atene CG, Martinelli S, Zucchini P, et al. IRF4 modulates the response to BCR activation in chronic lymphocytic leukemia regulating IKAROS and SYK. Leukemia 2021;35:1330–43.

Mareschal S, Pham-Ledard A, Viailly PJ, Dubois S, Bertrand P, Maingonnat C, et al. Identification of somatic mutations in primary cutaneous diffuse large B-cell lymphoma, leg type by massive parallel sequencing. J Invest Dermatol 2017;137:1984–94.

Nihira K, Ando Y, Yamaguchi T, Kagami Y, Miki Y, Yoshida K. Pim-1 controls NF-κappaB signalling by stabilizing RelA/p65. Cell Death Differ 2010;17:689–98.

Pham-Ledard A, Cappellen D, Martinez F, Vergier B, Beylot-Barry M, Merlio JP. MYD88 somatic mutation is a genetic feature of primary cutaneous diffuse large B-cell lymphoma, leg type. J Invest Dermatol 2012;132:2118–20.

Rogozin IB, Pavlov YI. The cytidine deaminase AID exhibits similar functional properties in yeast and mammals. Mol Immunol 2006;43:1481–4.

Sugimoto M, Tahara H, Ide T, Furuichi Y. Steps involved in immortalization and tumorigenesis in human B-lymphoblastoid cell lines transformed by Epstein-Barr virus. Cancer Res 2004;64:3361–4.

Willemze R, Cerroni L, Kempf W, Berti E, Facchetti F, Swerdlow SH, et al. The 2018 update of the WHO-EORTC classification for primary cutaneous lymphomas [published correction appears in Blood 2019;134:1112]. Blood 2019;133:1703–14.

Wilson WH, Young RM, Schmitz R, Yang Y, Pittaluga S, Wright G, et al. Targeting B cell receptor signaling with ibrutinib in diffuse large B cell lymphoma. Nat Med 2015;21:922–6.

Zhou XA, Louissaint A Jr, Wenzel A, Yang J, Martinez-Escala ME, Moy AP, et al. Genomic analyses identify recurrent alterations in immune evasion genes in diffuse large B-cell lymphoma, leg type. J Invest Dermatol 2018;138:2365–76.

Zinzani PL, Quaglino P, Pimpinelli N, Berti E, Baliva G, Rupoli S, et al. Prognostic factors in primary cutaneous B-cell lymphoma: the Italian study group for cutaneous lymphomas. J Clin Oncol 2006;24:1376–82.

SUPPLEMENTARY MATERIALS AND METHODS

Antibodies and reagents

Antibodies used for immunolabeling are described in Supplementary Table S3. The human CD40L multimer kit was from Miltenyi Biotec (Paris, France). IL-2, IL-4, and IL-10 were supplied by PeproTech (Neuilly-sur-Seine, France). DAPI was from Fischer Scientific (Bordeaux, France). Ibrutinib was provided by Bio-Techne (Rennes, France).

Patient

Biopsy from the patient with primary cutaneous diffuse large B-cell lymphoma-leg type was collected in RPMI (Fischer Scientific) supplemented with 10% fetal bovine serum (Dominique Dutscher, Bernolsheim, France) and 1% penicillin–streptomycin (Fischer Scientific) at the Oncodermatology Department of Université de Bordeaux (Bordeaux, France). The patient provided written informed consent in accordance with the Declaration of Helsinki and national ethics rules. Our institutional review board approved the manipulation of primary cutaneous diffuse large B-cell lymphoma-leg type samples (CER-BDX-2022-18).

Mice xenografts

In vivo experiments were performed according to ethical criteria approved by the French Ministry of Agriculture (agreement APAFIS#29572-2021 020517035043, version 4). A 2-mm^3 piece of the fresh biopsy was subcutaneously grafted in the inguinal fat pad of a female immunodeficient NSG (NOD.Cg-Prkdc[scid]Il2rg[tm1Wjll]/SzJ) mouse from the animal facility aged 8 weeks. Tumor volume was determined weekly by measuring the length and width of the tumor with a caliper and calculating the volume using the following formula: $V = lw^2/2$, where l is the length, and w is the width. When the tumor volume reached 2,000 mm^3, the mouse was killed. After dissection, one half of the tumors were formalin fixed, and the other half was dissociated for cell culture. Different organs were removed and formalin fixed for immunohistochemistry experiments.

Cell line establishment

After dissection, the tumor was mechanically dissociated. The percentage of $CD19^{pos}$ and $CD20^{pos}$ cells was determined by flow cytometry. In the beginning, cells were cultured at a high density (1–2 million/ml) in RPMI 1640 containing 10% human serum AB (Institut de Biotechnologies Jacques Boy, Reims, France), 10% fetal bovine serum (Dominique Dutscher), 1 μg/ml CD40L, 20 ng/ml IL-2, 10 ng/ml IL-4, 50 ng/ml IL-10, and 1% penicillin–streptomycin for 45 days. Cytokines were then gradually removed from the culture medium, and the cells were routinely diluted at 0.5 million/ml with fresh culture medium three times a week for 2 years.

Flow cytometry

The percentage of B cells in the tumor or in the culture was estimated on the basis of $CD19^{pos}CD20^{pos}$ $CD45^{pos}$ cell surface expression by flow cytometry using Canto II cytometer (BD Biosciences, Le Pont-de-Claix, France) and DIVA (Data-Interpolating Variational Analysis) software.

Cell proliferation assay

Cell doubling time was determined using the CellTrace violet Cell proliferation Kit (Fisher Scientific) according to the manufacturer's instructions. Briefly, 10^6 cells were stained with carboxyfluorescein succinimidyl ester-violet (5 μM) for 20 minutes at 37 °C, and after rinsing in the culture medium, cells were seeded in six-well plates. Cell proliferation was followed for 6 days by measuring cell fluorescence ($\lambda ex = 405$ nm, $\lambda em = 450$ nm) by flow cytometry. Analyses were performed using FlowJo (version 10.8) software.

Immunohistochemistry

Immunostainings were performed on 3-μm thick formalin-fixed paraffin-embedded mice organ sections. Cells in culture were fixed with 4% formalin, pre-embedded in 2% agarose, and further embedded in a paraffin block. Protein expression was revealed using primary antibodies described in Supplementary Table S3 and Impress IgG polymer kit peroxidase (Vector Laboratories, Eurobio Scientific, Les Ulis, France) with 3'3-diaminobenzidine as a chromogen. Sections were then counterstained with hematoxylin (Vector Laboratories). Hematoxylin-Eosin-Saffron–stained sections were analyzed in parallel. Images were obtained using a NIKON Eclipse C1 microscope coupled with a camera NIKON DS-F12 and NIS BR imaging software, version 4.0 (Nikon, Champigny Sur Marne, France).

Cytotoxicity assay

To determine the half-maximal inhibitory concentration of ibrutinib, 20,000 ARSI or OCI-Ly3 (DMSZ, Braunschweig, Germany) cells per well were seeded in 96-well plates, with various concentrations of ibrutinib for 72 hours. Ibrutinib cytotoxicity was determined using the luminescent cell viability assay CellTiter-Glo Cell viability assay (Promega, Charbonnières-les-Bains, France). Luminescence levels were quantified using the FlexStation 3 (Molecular Devices, San Jose, CA). Results were analyzed using GraphPad Prism software, version 9 (Graphpad Software, San Diego, CA).

Multicolor FISH karyotyping

Metaphase chromosomes preparations were done using the standard protocol: incubation with 0.1 μg/ml Colcemid (Gibco, Waltham, MA) for 4 hours, hypotonic shock with 0.075M potassium chloride for 20 minutes at 37 °C, and fixation with cold Carnoy's fixative (3:1 (v:v) methanol to glacial acetic acid). At least three fixative changes were applied, and these cytogenetic pellets were stored in fixative at −20 °C until use.

A multicolor FISH experiment was conducted according to the manufacturer's instructions (MetaSystems, Compiègne, France) using 24XCyte kit on metaphase spreads. Briefly, slides with metaphase spreads were prepared 1 week before hybridization, and every slide was checked for metaphase concentration. Slides were rehydrated by decreasing ethanol series (100, 70, 50, 30%) and 0.1× saline-sodium citrate (SSC), then treated with 2× SSC at 70 °C for 30 minutes, and let cool down for the next 20 minutes. Finally, slides were transferred to 0.1× SSC, denatured in 0.07 M sodium hydroxide, passed in 0.1× SSC and 2× SSC at 4 °C, and dehydrated by increasing ethanol series. Each step was performed at room temperature for 1 minute, if not specified. Slides were let air dried before applying probe. Probe mixture was denatured by incubating at 75 °C

for 5 minutes, then put on ice briefly, and incubated at 37 °C for 30 minutes. Prehybridized probe was applied onto the denatured chromosome preparation and overlaid with a coverslip, sealed with rubber cement, and let hybridize for 3 days at 37 °C in a humidified chamber (ThermoBrite System, Abbott Molecular, Des Plaines, IL). Post-hybridization washes were realized in 0.4× SSC at 72 °C for 2 minutes, then in 2× SSC/0.05% Tween-20 for 3 minutes, and in PBS for the next 2 minutes at room temperature. Finally, slides were left air dried and mounted with Vectashield (Vector Laboratories) containing DAPI to counterstain metaphase spreads.

Metaphase finder and image acquisition were performed using the fluorescence-based microscopic scanning system Metafer (MetaSystems, Amplitech SAS, Compiegne, France). This scanning system is based on a fully motorized Axio Imager Z2 microscope (Zeiss, Rueil Malmaison, France) equipped with a motorized eight-slide scanning stage (Märzhäuser Wetzlar, Wetzlar, Germany) and high-resolution monochrome camera CoolCube 1m (MetaSystems). The slide scanning and automated multicolor FISH acquisition are performed using 40× objective and appropriate individual excitation and emission filter sets. Metaphase images were then treated and analyzed manually with Isis software (MetaSystems) to establish karyotypes. We have acquired and collected a maximum of abnormal karyotypes (between 10 and 30 karyotypes) per sample, especially if two or more cytogenetic subclones were present. We define a subclone as an abnormal karyotype present at least in three metaphases.

Nucleic acid extraction

DNA and RNA were extracted using the QiAmp DNA mini kit (Qiagen, Hilden, Germany) and the Direct-Zol RNA miniprep kit (Zymo Research, Ozyme, Saint-Cyr l'Ecole, France), respectively, according to manufacturers' inst ructions.

Ig rearrangements

For evaluation of B-cell clonality, the human Ig rearrangements were studied using the BIOMED-2 protocol as described previously (van Dongen et al., 2003).

SNP array

DNAs extracted from the initial tumor of the patient and ARSI cell line were analyzed using BeadChip Infinium CytoSNP-8x850K, version 1.2 (Illumina, Évry, France), which contains nearly 850,000 SNPs with a 15× redundancy, giving an overall effective resolution of approximately 18 kb. Briefly, DNAs were amplified, fragmented, precipitated, and hybridized on the microarray before sample extension and staining, according to the manufacturer's instructions. Then, the microarray was scanned on the Next Seq 550Dx (Illumina), and the analysis was performed using BlueFuse Multi Software. Analyses were retained if the call rate was >0.955. For aberration analysis, we used the log R ratio parameter (on the basis of intensity information) in combination with the B-allele frequency metric (on the basis of the genotype information) providing powerful data and allowing us to detect copy-neutral loss of heterozygosity. The validated aberrations are presented according to International System for Human Cytogenomic Nomenclature 2020 standard.

Targeting next-generation sequencing using a lymphopanel

A lymphopanel was designed to identify alterations within 36 genes important for lymphomagenesis on the basis of literature data and on whole-exome sequencing of relapsed/refractory diffuse large B-cell lymphoma sequencing and previously used to characterize a primary cutaneous large B-cell lymphoma, leg type cohort (Ducharme et al., 2019; Mareschal et al., 2017). The lymphopanel was designed with Ion Ampliseq technology (Fisher Scientific) and covered 75.08 kb. These genes include *ARID1A, B2M, BCL2, BRAF, BTK, CARD11, CCND3, CD58, CD79A, CD79B, CDKN2A, CDKN2B, CIITA, CREBBP, CXCR4, EP300, EZH2, FOXO1, GNA13, ID3, IRF4, MEF2B, MYC, MYD88, NOTCH1, NOTCH2, PIM1, PLCG2, PRDM1, SOCS1, STAT6, TCF3, TNFAIP3, TNFRSF14, TP53,* and *XPO1*. Amplified libraries were sequenced with the IonS5 on 530 Chips, and data analysis was performed with Torrent Suite software, version 5.10 (Fisher Scientific). Reads were mapped to the human hg19 reference genome. The Variant Caller detected point mutations with a variant allele frequency ≥2% for single nucleotide variation and ≥5% for short insertion/deletion. Variant Call Format files were annotated by ANNOVAR (Wang et al., 2010). BAM sequences were also checked if necessary using Alamut Visual Software (SOPHiA Genetics, Saint-Sulpice, Swit zerland).

RNA sequencing

Library preparation, capture, seq uencing, and alignment have been done by IntegraGen SA (Evry, France). Libraries were prepared with NEBNext Ultra II Directional RNA Library Prep Kit (New England Biolabs, Evry, France) for Illumina protocol according to supplier instructions. mRNA molecules using poly-T oligo attached magnetic beads from 100 ng total RNA (with the Magnetic mRNA Isolation Kit from New England Biolabs) were purified and fragmented using divalent cations under elevated temperature. Cases were sequenced in pooled libraries on the NovaSeq6000 platform (paired-end 100 bp reads, Illumina).

Preprocessing. The quality of reads was assessed for each sample using FastQC (version 0.11.4). RNA-sequencing reads were aligned to GRCh38 using the STAR aligner (version 2.7.10a) (Dobin et al., 2013). The number of reads associated with each gene in the Gencode annotation, version 31, was obtained. Data normalization was performed with the Bioconductor DESeq2 package (Love et al., 2014) to import raw counts for each sample into R statistical software, version 4.1.2, and extracted the count matrix.

Clustering. We used the Bioconductor edgeR package (version 3.36.0) for differential analysis of sequence read count data. The normalized expression matrix from the 1,000 most variant genes (based on SD) was used to classify the samples according to their gene expression patterns. We used FactoMineR to perform Hierarchical Clustering on Principle Components (with euclidean distance and ward's method).

Gene set enrichment analysis. Preranked analysis was performed using the gene set enrichment analysis software, version 4.1.0, to calculate the normalized enrichment score and false discovery rate (Subramanian et al., 2005). A normalized enrichment score corresponds to the enrichment score, which reflects the degree to which a gene set is overrepresented at the top or bottom of a ranked list of genes. The normalization is based on the gene-set enrichment scores for all dataset permutations. Genes were preranked according to *t*-test statistic value obtained, thanks to limma R package. Gene sets that obtained the highest normalized enrichment score with a normalized $P < 0.005$, a false discovery rate < 0.005, and a Family-wise error rate $P < 0.045$ were considered significantly enriched. We used the Kyoto Encyclopedia of Genes and Genomes and custom *NFKB* gene list (Compagno et al., 2009) and a B-cell receptor gene list.

SUPPLEMENTARY REFERENCES

Compagno M, Lim WK, Grunn A, Nandula SV, Brahmachary M, Shen Q, et al. Mutations of multiple genes cause deregulation of NF-kappaB in diffuse large B-cell lymphoma. Nature 2009;459:717–21.

Dobin A, Davis CA, Schlesinger F, Drenkow J, Zaleski C, Jha S, et al. STAR: ultrafast universal RNA-seq aligner. Bioinformatics 2013;29:15–21.

Ducharme O, Beylot-Barry M, Pham-Ledard A, Bohers E, Viailly PJ, Bandres T, et al. Mutations of the B-cell receptor pathway confer chemoresistance in primary cutaneous diffuse large B-cell lymphoma leg type. J Invest Dermatol 2019;139:2334–2342.e8.

Love MI, Huber W, Anders S. Moderated estimation of fold change and dispersion for RNA-seq data with DESeq2. Genome Biol 2014;15:550.

Mareschal S, Pham-Ledard A, Viailly PJ, Dubois S, Bertrand P, Maingonnat C, et al. Identification of somatic mutations in primary cutaneous diffuse large B-cell lymphoma, leg type by massive parallel sequencing. J Invest Dermatol 2017;137:1984–94.

Subramanian A, Tamayo P, Mootha VK, Mukherjee S, Ebert BL, Gillette MA, et al. Gene set enrichment analysis: a knowledge-based approach for interpreting genome-wide expression profiles. Proc Natl Acad Sci USA 2005;102:15545–50.

van Dongen JJM, Langerak AW, Brüggemann M, Evans PAS, Hummel M, Lavender FL, et al. Design and standardization of PCR primers and protocols for detection of clonal immunoglobulin and T-cell receptor gene recombinations in suspect lymphoproliferations: report of the BIOMED-2 Concerted Action BMH4-CT98-3936. Leukemia 2003;17:2257–317.

Wang K, Li M, Hakonarson H. ANNOVAR: functional annotation of genetic variants from high-throughput sequencing data. Nucleic Acids Res 2010;38:e164.

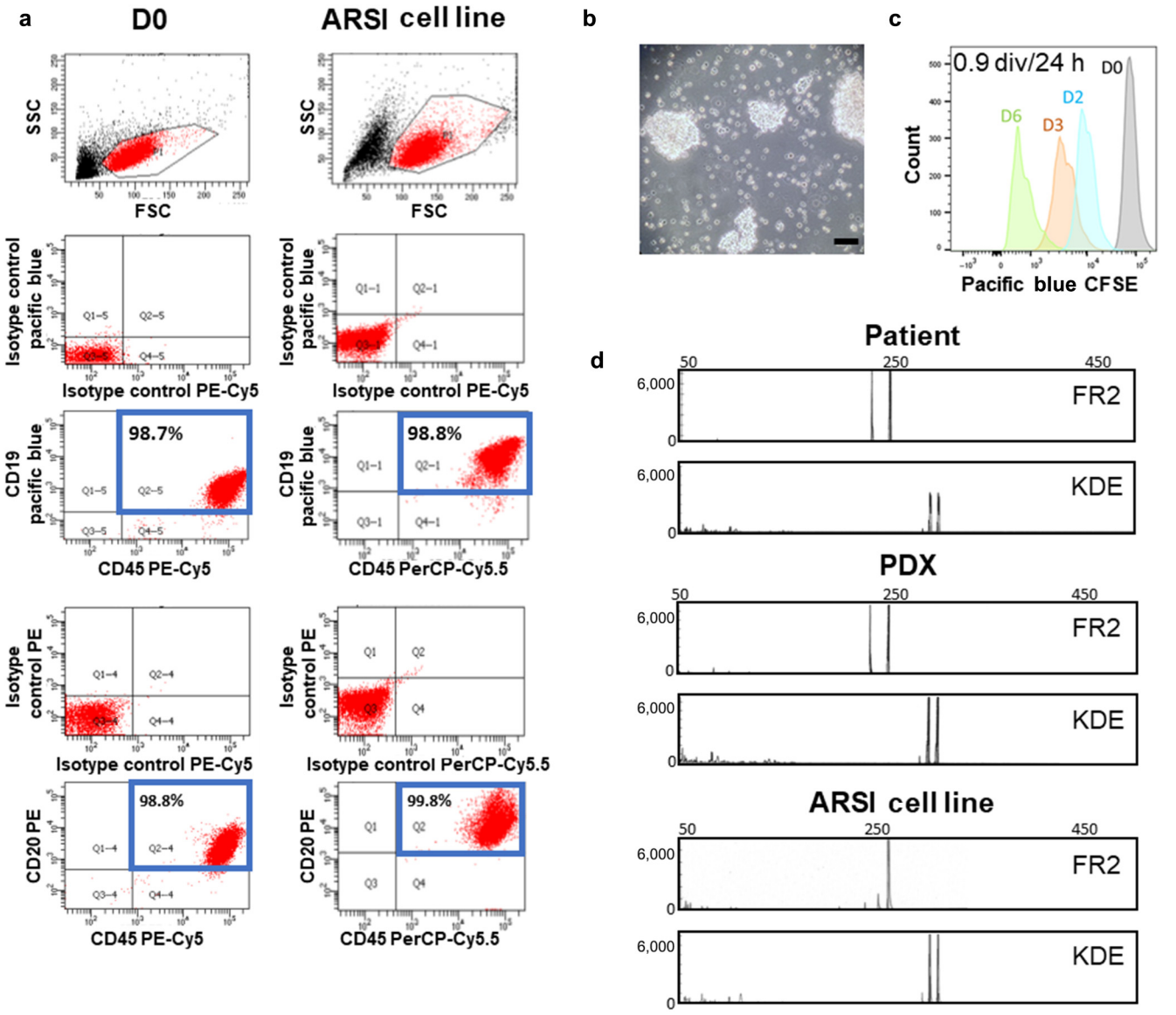

Supplementary Figure S1. Characteristics of ARSI cell line. (**a**) Immunophenotype of cells from PDX (D0) and ARSI cell line after 7 months in culture according to CD45, CD20, and CD19 expression determined by flow cytometry. (**b**) Phase-contrast image of ARSI cells growing in aggregates in culture medium. Bar = 50 μm. (**c**) Tracking cell division using CFSE staining. Representative flow cytometry analysis of CFSE staining on days 2, 3, and 6. Cell generations were identified according to cell staining on D0 using FlowJo software. (**d**) Ig rearrangement between the original patient tumor, PDX, and ARSI cell line (11 months) was determined by the BIOMED-2 protocol. CFSE, carboxyfluorescein succinimidyl ester; D, day; div, division; FSC, forward scatter; PDX, patient-derived xenograft; PE, phycoerythrin; Q, quartile; SSC, side scatter.

Supplementary Table S1. mFISH and SNParray Analyses of Patient Tumor and Patient-Derived Cell Line According to Time in the Culture

Sample	SNP Array	mFISH Karyotype
Patient tumor	arr[GRCh37]2q24.32q34(164485597_210073419)x1, 3p21.31-p14.3(49441091_58232485)x1, 6pter-p25.2(108666_2832331)x1, 7q31.31-q36.3(118850537_159124481)x1, 9p21.3(21728683_21979204x1,21984661_22056499x0), 9p21.3-p21.2(22077543_25717386)x1, 14q24.1(68370656_68692290)x0, 14q32.33(106082680_107078986)x1, 18x3, 19q12q13.43(30090883_59095126)x3, Xq28(148561332_155236747)x3	Not available
ARSI 7 mo	arr[GRCh37]2q24.3q34(164436645_210077614)x1, 3p21.31p14.3(49389842_58228082)x1, 6p25.3-p25.2(304135_2842830)x1, 7p21.3p14.3(11394751_35247446)x2 mos hmz, 7q31.31q36.3(118701195_159126310)x1, 9p21.3(21728683_21944317x1,21944818_22062134x0), 9p21.3-p21.2(21062134_25717537)x1, 14q24.1(68370656_68711163)x0, 14q32.33(106082680_107083638)x1, 18x3, 19q12q13.43(29808196_59036479)x3, Xq28(148562599_155141985)x3	47, XX, der(2)del(2q)(WCP2+), der(3)t(3;12)(WCP12+,WCP3+), der(6)add(6)(q2?6)(WCP6+,WCP19+), der(7)t(7;12)(WCP7+,WCP12+), der(12) t(3;12)(WCP3+,WCP12+),+18 [21]
ARSI 13 mo	arr[GRCh37]2q24.3-2q34(164965571_210118415)x1, 3p21.31-p14.3(49317338_58278244)x1, 6pter-p25.2(108666_2876581)x1, 7p21.3p14.3(63494_34283049)x2 mos hmz, 7q31.31-q36.3(119270386_15926310)x1, 9p21.3(21728683_21944317x1,21944818_22062134x0),9p21.3-p21.2(21062134_25745702)x1, 14q24.1(68413835_68793554)x0, 14q32.33(106079698_107242489)x1, 18x3,19q12qter(29262931_59097160)x3, Xq28(148525485_155236747)x3	46∼48,X[6], +X[13], der(2)del(2q) (WCP2+)[19], der(3)t(3;12) (WCP12+,WCP3+)[19], der(6)add(6)(q2?6)(WCP6+,WCP19+)[19], der(7)t(7;12)(WCP7+,WCP12+)[19], der(12) t(3;12)(WCP3+,WCP12+)[19], +18[19],+18[8][cp19]

Abbreviation: mFISH, multicolor FISH.

Supplementary Table S2. List of the Somatic Mutations Detected by the Lymphopanel

Gene	Transcript	Mutation	Initial Tumor, %	D0, %	7 mo, %	11 mo, %
CD79B	NM_000626.3	c.587A>G ; p.(Tyr196Cys)	34	46	52	47
IRF4	NM_002460.3	c.166C>T ; p.(His56Thr)[1]	20	/	/	/
		c.178C>A ; p.(Gln60Lys)[1]	/	/	/	53
		c.312C>A ; p.(Ser104Arg)[1]	/	/	100	100
MYD88	NM_002468.4	c.794T>C ; p.(Leu265Pro)	36	55	49	50
PIM1	NM_001243186.1	c.367G>C ; p.(Glu123Gln)	43	51	52	50
		c.370C>T ; p.(Pro124Ser)	31	48	48	50
		c.475C>T ; p.(His159Tyr)	26	33	43	37
		c.497C>T ; p.(Ser166Phe)[1]	55	95	96	96
		c.658C>G ; p.(Leu220Val)	36	52	96	94
		c.676G>A ; p.(Glu226Lys)	/	/	100	100

Abbreviations: AID, activation-induced cytidine deaminase; aSHM, aberrant somatic hypermutation; D0, day 0; DLBCL, diffuse large B-cell lymphoma; SNV, single nucleotide variation; WES, whole-exome sequencing.

This shows the 36 genes involved in lymphomagenesis on the basis of literature data and WES of relapsed/refractory DLBCL.

[1]SNV targeted by aSHM located at DGYW/WRCH AID target sites at diagnosis.

Supplementary Table S3. List of Antibodies Used for Flow Cytometry and Immunohistochemistry

Antibody	Supplier	Clone	pH	Dilution
Antibodies for flow cytometry				
Mouse anti-humanCD19-BV421	BD Biosciences (Le pont de Claix, France)	HIB19	Not applicable	1/50
Mouse anti-human CD20-PE	BD Biosciences (Le pont de Claix, France)	2H7	Not applicable	1/50
Mouse anti-human CD45-PECy5.5	BD Biosciences (Le pont de Claix, France)	J.33	Not applicable	1/50
Antibodies for Immunohistochemistry				
Mouse monoclonal anti-HLA-ABC	Abcam (Paris, France)	EMR8-5	6	1/100
Mouse monoclonal anti-human CD20	Agilent (Les Ullis, France)	L.26	9	1/300
Mouse monoclonal anti-human MUM1	Agilent (Les Ullis, France)	MUM1p	9	1/100
Mouse monoclonal anti-human BCL2	Agilent (Les Ullis, France)	124	6	1/200
Rabbit monoclonal anti-C-MYC	Abcam (Paris, France)	Y69	9	1/50
Rabbit polyclonal Anti-IgM	Roche (Rotkreuz, Switzerland)		6	Ready to use
Rabbit polyclonal Anti-IgG	Roche (Rotkreuz, Switzerland)		6	Ready to use
Mouse monoclonal anti-Ki-67	Agilent (Les Ullis, France)	MIB-1	9	1/300
Mouse monoclonal anti-BCL6	Agilent (Les Ullis, France)	PG-B6p	9	1/25
Mouse monoclonal anti-human CD10	Thermo Fisher Scientific (Illkirch-Graffenstaden, France)	56C6	9	1/20

Abbreviations: BV, brilliant violet; Cy, cyanine; PE, phycoerythrin.